NUMERICAL STUDY OF LAKE-LAND BREEZE OVER LAKE VÄTTERN SWEDEN

Wu Zengmao

NUMERICAL STUDY OF LAKE-LAND BREEZE
OVER LAKE VÄTTERN SWEDEN

Wu Zengmao

Author (s)

Wu Zengmao

Title (and Subtitle)

NUMERICAL STUDY OF LAKE-LAND BREEZE OVER LAKE VÄTTERN SWEDEN

Abstract

This paper describes a two-dimensional lake breeze model with turbulent energy closure. The simulated results show that (1) the front of the lake breeze progresses inland faster in the late afternoon than at the fully developed stage; (2) the lake breeze and land breeze have larger extension offshore than inland. The acceleration of the front in the declining phase of the lake breeze is explained in terms of the decreased turbulent friction acting on the head of the lake breeze. The larger extension offshore, probably, is attributed to the smaller roughness of water surface and to the offshore synoptic wind.

Key words

breeze front
declining phase
fully developed stage
lake breeze
land breeze
onset

Report available from:

CONTENTS   Page

1. INTRODUCTION

This paper describes the results of numerical study of a lake-land breeze and related diurnal variations. A case has been simulated, which occured over Lake Vättern, Sweden (shown in Figure 1), on 7-8 May 1980. The data of GOTEX II experiment (Bergström and Alexandersson 1981, Ericson 1982) have been used.

The model essentially is a modification of a two-dimensional, hydrostatic primitive equation model with turbulent energy closure which was presented by Bodin et al. (1980) and Melgarejo (1980). The modification involves the following changes: (1) Separating the mesoscale variables from the large scale, dependent variables; (2) improvement of the mixing length formulation; (3) inclusion of a prediction equation for the height of the planetory boundary layer.

The inland advance rate of the front of the lake breeze, calculated with this model, shows some interesting features consistent with the observations and calculations made by Simpson (1977) and Physick (1980). The turbulent energy closure scheme makes it possible to realistically estimate the turbulent diffusion coefficient and to find a relation between the progression of the front and turbulent friction acting on the lake breeze head, as well as further to explain these features.

2. NUMERICAL MODEL

In deriving the equations of the model, the dependent variables are decomposed as

$$A = \bar{A} + a + a'$$

where A represents any one of U, V, W, Θ and Π. The barred component denotes the large (synoptic) value. The primed one indicates the value on a scale that is too small to be resolved explicitly by the model grid and whose effect must be parameterized. The value represented with a lowercase letter denotes the mesoscale variable, which is defined as a deviation from the synoptic state, and which is of primary interest in this case. It is assumed that the atmosphere is incompressible and in hydrostatic equilibrium, and that the large scale fields ($\bar{U}$, $\bar{V}$ and $\bar{\Theta}$) are steady and homogeneous along both horizontal directions, $\bar{W} = 0$. The mesoscale field is assumed to be homogeneous in the y direction. In addition, topography and humidity have not been taken into account in the model. x is west-east; y south-north.

2.1 Governing equations

$$\frac{\partial u}{\partial t} + (\bar{U} + u)\frac{\partial u}{\partial x} + w\left(\frac{\partial \bar{U}}{\partial z} + \frac{\partial u}{\partial z}\right) = f(\bar{V} + v - \bar{V}_{gR}) - \frac{\partial \pi}{\partial x}$$

$$+ \frac{\partial}{\partial z}\left(K_m\left(\frac{\partial \bar{U}}{\partial z} + \frac{\partial u}{\partial z}\right)\right)$$

$$\frac{\partial v}{\partial t} + (\bar{U} + u)\frac{\partial v}{\partial x} + w\left(\frac{\partial \bar{V}}{\partial z} + \frac{\partial v}{\partial z}\right) = -f(\bar{U} + u - \bar{U}_{gR})$$

$$+ \frac{\partial}{\partial z}\left(K_m\left(\frac{\partial \bar{V}}{\partial z} + \frac{\partial v}{\partial z}\right)\right)$$

$$\frac{\partial \theta}{\partial t} + (\bar{U} + u)\frac{\partial \theta}{\partial x} + w\left(\frac{\partial \bar{\theta}}{\partial z} + \frac{\partial \theta}{\partial z}\right) = \frac{\partial}{\partial z}\left(K_H\left(\frac{\partial \bar{\theta}}{\partial z} + \frac{\partial \theta}{\partial z} - \Upsilon_{cg}\right)\right)$$

$$\frac{\partial w}{\partial z} + \frac{\partial u}{\partial x} = 0$$

Exner function Π, is defined as

$$\Pi = \theta \, C_p \, (P/P_0)^{R_d/C_p} \qquad P_0 = 1000 \text{ mb}$$

$$\frac{\partial \pi}{\partial z} = g \, \theta/\bar{\theta}$$

$$\bar{V}_{gR} = \frac{1}{f}\frac{\partial \bar{\pi}}{\partial x} = \frac{1}{f}\frac{\partial \bar{\pi}}{\partial x}\Big|_H = \text{constant}$$

$$\bar{U}_{gR} = -\frac{1}{f}\frac{\partial \bar{\pi}}{\partial y} = -\frac{1}{f}\frac{\partial \bar{\pi}}{\partial y}\Big|_H = \text{constant}$$

Where Υ_{cg} is the counter-gradient heat flux correction, the rest of the symbols have their normal meaning in meteorological parlance. Υ_{cg} is calculated with

$$\gamma_{cg} = \begin{cases} -C_r \cdot u_* \cdot \Theta_*/(w_* \cdot h) & \Theta_* < 0 \\ 0 & \Theta_* \geq 0 \end{cases}$$

and γ_{cg} keeps the value below 0.003 (K/m). w_* is convective scaling velocity. Its value is given by

$$w_* = \begin{cases} (-\frac{g}{(\bar{\Theta} + \Theta)_s} \cdot u_* \cdot \Theta_* \cdot h)^{1/3} & \Theta_* < 0 \\ 0 & \Theta_* \geq 0 \end{cases}$$

where u_* is surface friction velocity, Θ_* surface friction temperature. The subscript "s" indicates surface properties. C_r is taken as 5 (Therry et al., 1983). h is the height of the planetary boundary layer and predicted with a prognostic equation based on Deardoff's (1974) work.

$$\frac{\partial h}{\partial t} + (\bar{U} + u) \frac{\partial h}{\partial x} - w|_h = (1.8 \, (w_*^3 + 1.1 \, u_*^3 - 3.3 \, u_*^2 \cdot f \cdot h))$$

$$/(g \cdot h^2 / \bar{\Theta}_s \cdot \frac{\partial (\bar{\Theta} + \Theta)^+}{\partial z} + 9 \, w_*^2 + 7.2 \, u_*^2)$$

and where $\partial (\bar{\Theta} + \Theta)^+/\partial z$ describes the lapse rate of potential temperature above h.

The reason for choosing this formulation, which is really an over-specification of h, instead of a diagnostic equation, is really numerical. When going through the integration a diagnostic equation gives very low h-values near the coastline, which sometimes have a detrimental effect on the simulation.

K_m and K_H are the turbulent diffusivities for momentum and heat. K_m is specified:

$$K_m = l \cdot (\alpha_1 E)^{1/2}$$

l is mixing length, E turbulent kinetic energy.

$E = \frac{1}{2} \, (\overline{u'^2} + \overline{v'^2} + \overline{w'^2})$, and the ratio $\alpha_H = K_H/K_m = 1.35$ is utilized. The equation of E is expressed (Bodin, 1979) as:

$$\frac{\partial E}{\partial t} + (\bar{U} + u) \frac{\partial E}{\partial x} + w \frac{\partial E}{\partial z} = K_m \, (S_v^2 - \alpha_H \, g/\bar{\Theta} \, (\frac{\partial \bar{\Theta}}{\partial z} + \frac{\partial \Theta}{\partial z} - \gamma_{cg}))$$

$$+ \alpha_2 \frac{\partial}{\partial z} \, (K_m \frac{\partial E}{\partial z}) - \varepsilon$$

and

$$S_v^2 = (\frac{\partial \bar{U}}{\partial z} + \frac{\partial u}{\partial z})^2 + (\frac{\partial \bar{V}}{\partial z} + \frac{\partial v}{\partial z})^2$$

where ε is turbulent kinetic energy dissipation.

$\varepsilon = (\alpha_3 E)^{3/2}/l_\varepsilon$; and $\alpha_1 = 0.2$, $\alpha_2 = 1.2$, $\alpha_3 = 0.2$. l_ε is the dissipation mixing length. l and l_ε are formulated similarly as Therry (1983) did.

2.2   Initial conditions

The case of the lake-land breeze over Lake Vättern, on 7-8 May 1980, is chosen for simulation. During the period, the weather was clear and a stationary anticyclone controlled the area studied. A south-easterly wind was prevailing in low levels.

The simulation starts at 2000 local time of May 6. The synoptic potential temperature profile is obtained by averaging four radiosonde ascents at 02, 08, 14, 20 local time of May 7. The synoptic wind ($\bar{U}$ and $\bar{V}$) is obtained with an one-dimensional dynamic model with nudging (Hoke and Anthes, 1976). It is assumed that at t=0, $u=v=w=\Theta=\Pi=0$. The initial value of turbulent kinetic energy is calculated diagnostically, based on the assumption of balance between the production and dissipation of turbulent energy.

$$E = 5 \, l^2 \cdot S_v^2 \, (1 - \alpha_H R_i)$$

R_i is the gradient Richardsson number. The initial value of h is estimated according to the synoptic potential temperature profile and the starting time of the simulation.

2.3   Boundary conditions

It is assumed that at $z=z_0$, $u=v=w=0$. Since a staggered grid is used, we have at the bottom of the grid for eddy energy, $\frac{\partial E}{\partial z} = 0$ and for temperature a constant $8.1^\circ C$ at the lake surface and a prescribed diurnal temperature wave $F_s(x,t)$ at the land surface. $F_s(x,t)$ is obtained from the hourly screen observation (at Klockrike) and shown in Figure 2. Meanwhile an advective temperature correction is added to the grid-points near the coastlines.

The top of the model domain, H is taken as 3000 m, and at z=H, $\frac{\partial u}{\partial z} = \frac{\partial v}{\partial z} = \frac{\partial E}{\partial z} = \Theta = \pi = 0$. L is the horizontal extent of the model domain; x=0 and x=L $\frac{\partial \Theta}{\partial x} = 0$, and the so-called "constant inflow and gradient outflow" contidions are utilized for equations of u, v and E. An implicit filter enhanced near the lateral boundaries is employed to prevent contamination of the inner domain.

The surface roughness parameter is simply set as 0.15, 0.10 and 0.0001 m for the western and eastern coast area and water surface respectively.

2.4 Numerical integration

The integration domain is 3 km × 127.5 km, 43 gridpoints in the horizontal direction and 30 gridpoints in the vertical direction. The grid interval for x is 3 km uniformly. In order to get greater resolution near the ground, a coordinate transformation in vertical direction has been employed

$$\zeta = D(\frac{1}{K} \ln (z+z_D/z_D) + z/\lambda) + C_0$$

K = 0.35, von Karman constant; z_D = 0.3 m, λ = 0.2 H; and C_0 = 1 for u, v and Π, C_0 = 0.5 for the others. D is specified by using z = H, ζ = 30. A staggered grid in x and z directions is introduced to minimize the numerical error in the diagnostic equaitons and phase speed distortion of the internal gravity waves.

To approximate the vertical diffusive terms, a fully implicit finite difference scheme, a Laasoner scheme is employed. The forward-time scheme and the linear interpolation upstream scheme are utilized for time difference and advective terms respectively.

3. RESULTS

The simulated results show that the lake breeze starts at about 1000 hours, and gets in its fully developed stage at about 1600 hours. In the next 5 hours the lake breeze still prevails but reduces its intensity and by 2130 hours the breeze has collapsed at ground and gradually extends upwards. At about 0100 of the next day the land breeze appears firstly around the eastern shore, and by 0630 it gets in the strongest stage.

To notice that, when figures are discussed, '*' denotes the site of GOTEX II experiment; 'I ..... I' indicates the lake area.

3.1 Characteristics of the lake breeze circulation

It can be seen from Table 1 that variation in time of wind at the western shore is reproduced reasonably well, and that the observed results confirm the onset of the lake breeze at about 1000 local time.

TABLE 1. Variation in time of wind direction (WD) and speed (WS) on 7 May 1980 (Karlsborg at 10 metres).

Local time (hrs)	Calculated		Observed	
	WS m/s	WD	WS m/s	WD
08	5.0	137	3.3	170
09	4.9	131	1.6	130
10	4.6	122	2.5	70
11	4.0	117	1.8	100
12	3.3	114	2.0	130
13	2.7	114	2.2	120
14	2.1	116	2.0	120
15	1.6	124	2.0	100
16	1.3	130	2.0	*
17	1.2	106	3.0	65
18	1.3	88	3.0	65
19	1.5	86	5.6	90
20	2.0	86	5.8	110
21	2.4	100	4.7	120
22	3.0	129	3.0	110

*) = no record

Figure 4 and 5 present the features of the lake breeze circulation when it is in the fully developed stage. We can see that the branch located at the western coast is much weaker than one at the eastern coast. This is due to that the easterly prevailing wind at low level advects the colder lake air into the western land, and prevents the development of the breeze. We can see from Figure 4 that the lake breeze extends offshore farther than inland. A similar phenomenon is also found in the land breeze simulated. Estogue's (1976) results have the same feature. Perhaps, it can be attributed to both a offshore synoptic wind and a smaller drag force at the water surface than at land. To notice the location of the inland front (in Table 2) and the center of the vertical velocity maximum (Figure 6), we can find that the center is formed basically over the front and located at 400-700 m level, and moves following the front; in comparison, the center of the lake breeze maximum is almost standing and located at about 100 m from ground.

The calculated results illustrate that the mesoscale flow gradually veers clockwise, and the component parallell to the coastline can prevails over that one normal to the coastline in the late afternoon. Figure 7 shows the vertical structure of the component parallell to the coastline at 2000 hours, when it gets in the strongest stage.

In addition, Figure 8 and 9 demonstrate that the observed wind profiles (at Klockrike) at different times are reproduced satisfyingly, especially the simulation of the V component and the low-level jetstream at night are rather nice. However, the profiles of the U component at 17 hours present a 6 m/s difference at 120 m level, we believe that it might be attributed to the uncertainty in the observed data.

3.2　Inland advance rate of the lake breeze front

Following the identification of three types of the sea breeze front, the second type is a wind-shift line, as reported by Fosberg and Schroeder (Atkinson, 1981, pp 152). We take the leading line of the gradient maximum of u as the front, which mostly is consistent with zero line of the compositive component U. It is worth noticing that in the following discussion of this subsection, we limited ourself to the inland front of the lake breeze located at the eastern shore.

TABLE 2. Variation in time of position of the front, potential temperature difference $(\Theta_L(t) - \Theta_B(t))$ and K_f. Fx is the distance from the eastern shoreline. Θ_L and Θ_B denote the potential temperature of the land and the breeze air. They are read from two points which are 3 km from the front respectively ahead and behind, and located at the same level as the center of the breeze. K_f is the averaged turbulent momentum diffusivity along the upper surface of the breeze head, and the value within parenthesis corresponds to the bottom of the breeze.

	Time (hours)					
	1230	1400	1530	1700	1830	2000
Fx (km)	3	5	7	9	15	21
$(\Theta_L - \Theta_B)$ (K)	1.0	1.0	0.8	0.6	0.5	0.3
K_f (m²/s)	180	200	130	80	0.6	0.005 (0.03)
$10^2 \cdot (f \cdot K_f)^{\frac{1}{2}}$	14.9	15.7	12.7	10.0	0.9	(0.2)

If the front is projected hour by hour onto the cross sections of turbulent momentum diffusivity K_m, it can be found that variation of the advance rate of the front is closely related to the values of K_m around the front. Table 2 shows that during 1230–1700 hours the front progresses 6 km. After that it advances 12 km in 3 hours. It is surprising that the more energetic the lake breeze is, the more slowly the front moves. So far this feature hasn't universally been confirmed, but has been observed and simulated by Simpson (1977), Neumann (1974) and Physick (1980). Figure 10 shows Physick's results. Simpson (1977) explained this phenomenon in terms of the increased temperature contrast at the front in the late afternoon. However the results of this model show a decreased temperature contrast, which is coincident with Rao's observation (Atkinson, 1981, pp 140), so we try to explain the feature in another way.

We suppose that the lake breeze head moves in balance with the pressure force and the drag force, as shown schematically in Figure 11. $\overline{F_p} + \overline{F_d} = 0$, and $\overline{F_d} = \overline{F_{d1}} + \overline{F_{d2}} + \overline{F_{d3}}$. $\overline{F_p}$ and $\overline{F_d}$, respectively, denotes pressure force and drag force which act on a unit width of the head. $\overline{F_{d1}}$ is the part of drag acting on the upper surface of the head, $\overline{F_{d2}}$ —— acting on the bottom boundary, $\overline{F_{d3}}$ —— lateral surface. Generally, $\overline{F_{d2}}$ is much smaller than $\overline{F_{d1}}$, the lateral surface length is far shorter than the upper surface as well, so that $\overline{F_{d1}}$ substitudes for $\overline{F_d}$ without losing reality. Additionally the results of the numerical experiment done by Pearson (Longhetto, 1980, pp 133) point out that the advance rate of a sea breeze front is reduced when Coriolis force is increased. Based on the above facts and dimensional analysis, the drag force can be written as

$$F_d = cu_1 \qquad c = \beta (f \cdot K_f)^{\frac{1}{2}}$$

The pressure force is expressed as

$$F_p = \int_l d \cdot g \cdot \frac{1}{\rho} \frac{\partial \rho}{\partial x} dx \simeq d \cdot g \cdot \Delta \rho / \rho$$

where l is the horizontal scale of the head, d the vertical size; u_1 is the relative speed in which the head moves with respect to the air ahead of the front. Using Boussinegue approximation $\Delta \rho / \rho \simeq - \Delta T / T \simeq (\Theta_L(t) - \Theta_B(t) / (\Theta_L + \overline{\theta})$ We obtain

$$u_1 = \alpha \cdot d \cdot g \cdot (f \cdot K_f)^{-\frac{1}{2}} \cdot (\Theta_L(t) - \Theta_B(t)) / (\Theta_L(t) + \overline{\theta})$$

U_f is the advance rate of the front. U_a is the x-direction speed of the air ahead of the front and estimated from U_{gR}. U_f is written as:

$$U_f = U_a + u_1$$

$\alpha = 1/\beta$ is an experimental constant. In this experiment the above formulas provide an estimation that α is 0.02-0.03.

In the late afternoon, however, to estimate u_1 seems to be rather complicated due to ground cooling and an inversion being formed near the ground. The vertical size of the head gets reduced and the head is isolated from the ground. Turbulence intensity in vicinity of the head gets weaker, and $\overline{F_{d1}}$ gets smaller than $\overline{F_{d2}}$. Meanwhile, the lake breeze air is heated by a smaller heat flux when penetrating inland. However, owing to being heated over a longer time than before, Θ_B is reduced less than Θ_L. Based on the formula and analyses above, we may conclude that the key reason for which the lake breeze penetrates fast in the late afternoon is the sharp reduction of the drag acting on the breeze head.

3.3   Transition from the lake breeze to the land breeze

The simulated results show that after sunset the lake breeze located at the eastern shore collapses and breaks down into two parts over the lake. The eastern part declines rapidly and disappears. The western part and the return current of the lake breeze descend. The

land breeze is formed at about 0100 hours, and with two centers. The one located at the western shore is based on the remainder of the lake breeze, another one is related to the return current. In the meantime the flow, parallel to the coastline and corresponding to the land breeze, occurs as well.

Figure 12 and 13 show the vertical structure of the land breeze circulation and potential temperature, when the breeze gets into its fully developed stage. The land breeze in (a) of Figure 12 appears a little stronger than in (b), mainly because the mesoscale flow field, from which the land breeze is generated, is somewhat different in two cases. We also can find that the strong inversion near the ground, especially the part related to the cold tongue over the lake, acts as a major damping mechanism on development of the land breeze. In fact, the land breeze circulation is restricted below the nocturnal jetstream of low level.

CONCLUSIONS

Generally, this model reproduces the lake-land breeze circulation realistically in comparison to some observed results. The numerical simulation brought out several interesting features. The most pronounced is that the inland advance rate of the lake breeze front at the fully developed stage is relatively small as compared to the declining phase. It appears that the turbulent viscous friction is the most important factor affecting the inland advance rate. The simulated results show that the lake and land breezes have larger extension offshore than inland. Perhaps this phenomenon can be attributed to the offshore synoptic wind and different roughness between water surface and land. However, further observational and theoretical verification is necessary. We also can conclude that the strong inversion near the ground, especially the part related to the cold tongue over the lake, acts as a major damping mechanism on development of the land breeze circulation, and the whole circulation is restricted below the low-level jetstream at night.

ACKNOWLEDGEMENTS

REFERENCES

Atkinson, B.W., 1981: Meso-scale Atmospheric Circulations (chapter 5). Academic Press, London.

Bergström, H. and Alexandersson, H., 1981: Atmospheric Boundary Layer Field Experiment in Sweden 1980, part II. Reports No. 65, Uppsala.

Bodin, S., 1979: A predictive Numerical Model of the Atmospheric Boundary Layer Based on the Turbulent Energy Equation. SMHI Report, RMK 13.

Bodin, S., Ericson, K. and Schoeffler, P., 1980: Where and how will a radioactive cloud from Barsebäck land? SMHI Report, FoU-notiser Nr 9.

Dalu, G.A. and Green, J.S.A., 1980: Energetics of diabatic mesoscale circulation: A numerical study. Quart. J.R. Met. Soc. 106, pp 727-734.

Ericson, K. 1982: Atmospheric Boundary Layer Field Experiment in Sweden 1980. Part I. SMHI Reports, RMK 33.

Estogue, M.A., Gross, J. and Lai, H.W., 1976: A Lake Breeze over Southern Lake Ontario.

Hoke, J.E. and Anthes, R.A., 1976: The initialization of numerical models by a dynamic-initialization technique. Mon. Weather Rev. 104, pp 1551-1556.

Longhetto, A. (Editor), 1980: Atmospheric Planetory Boundary Layer Physics (Chapter 1-3). Elsevier scientific publishing company.

Melgarejo, J., 1980: Numerical experiments of wind over Gotland with a two-dimensional mesometeorological boundary layer model. SMHI Report. FoU-notiser Nr 11.

Neumann, J. and Mahrer, Y., 1974: A theoretical study of the sea and land breeze of circular island. J. Atmos. Sci. 31, pp 2027-2039.

Physick, W.L., 1980: Numerical experiments on the inland penetration of the sea breeze. Quart. J.R. Met. Soc. 106, pp 735-746.

Pielke, R.A., 1984: Mesoscale Meteorological Modeling (Chapter 7, 11). Academic Press, INC.

Saito, N., 1976: Numerical experiments of the land and sea breeze circulation. Papers in Meteorology and Geophysics, Vol. 27, No. 4, pp 99-117.

Simpson, J.E., Mansfield, D.A. and Milford, J.R., 1977: Inland penetration of sea breeze fronts. Quart. J.R. Met. Soc. 103, pp 47-76.

Therry, G. and Lacarrére, P., 1983: Improving the eddy kinetic energy model for planetary boundary layer description. Bound. Layer Met. 25, pp 63-68.
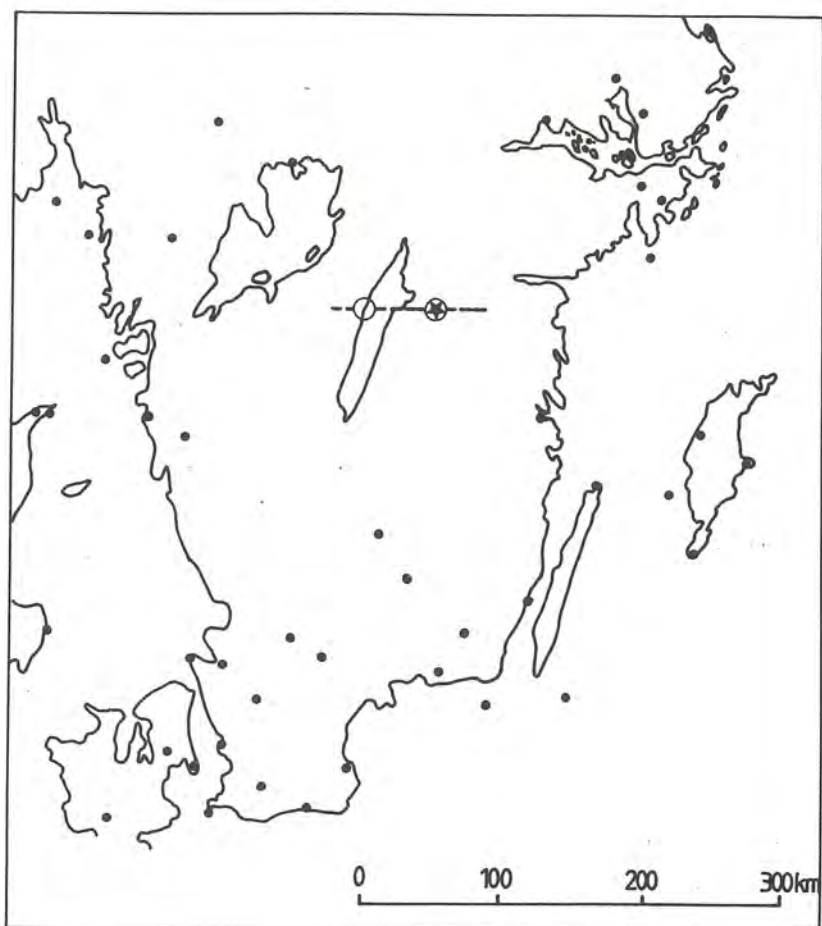
FIGURE 1. ⊛ denotes the experimental site, dashed line shows the cross section simulated and the mark 'O' the synoptic station Karlsborg.

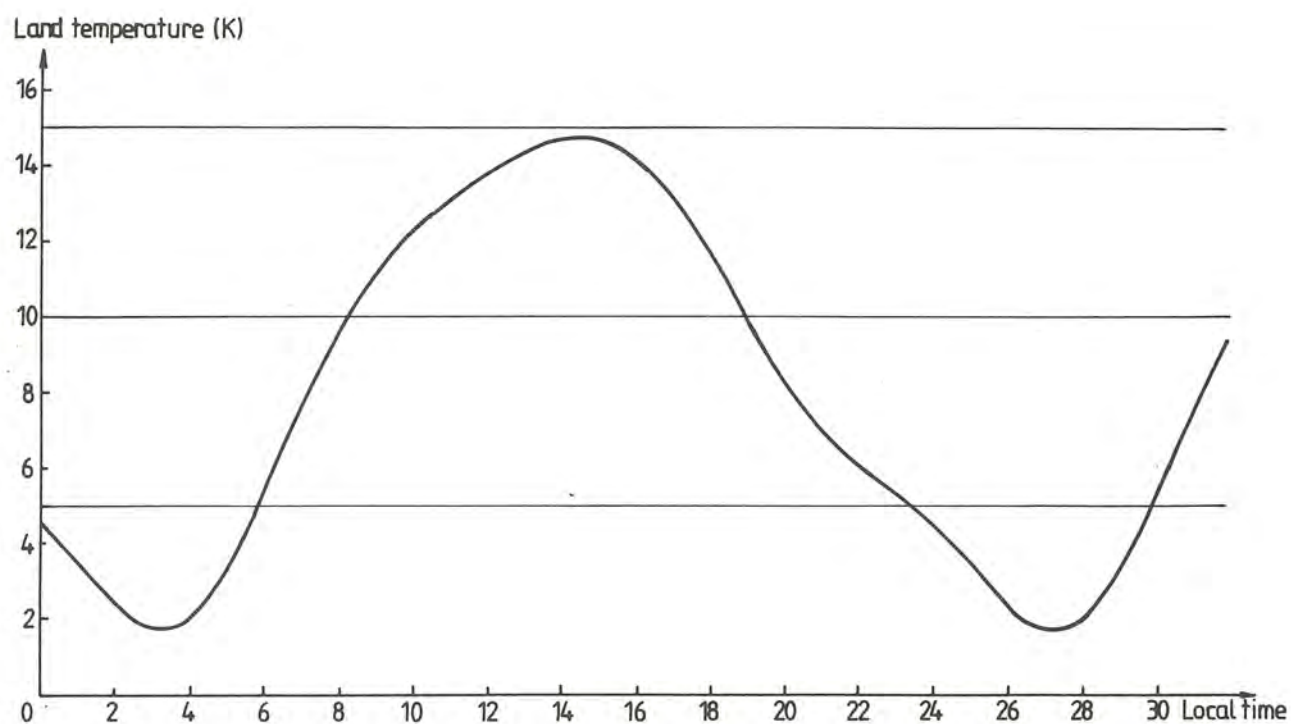FIGURE 2. Diurnal variation of the land surface temperature on May 7, 1980 (at Klockrike).
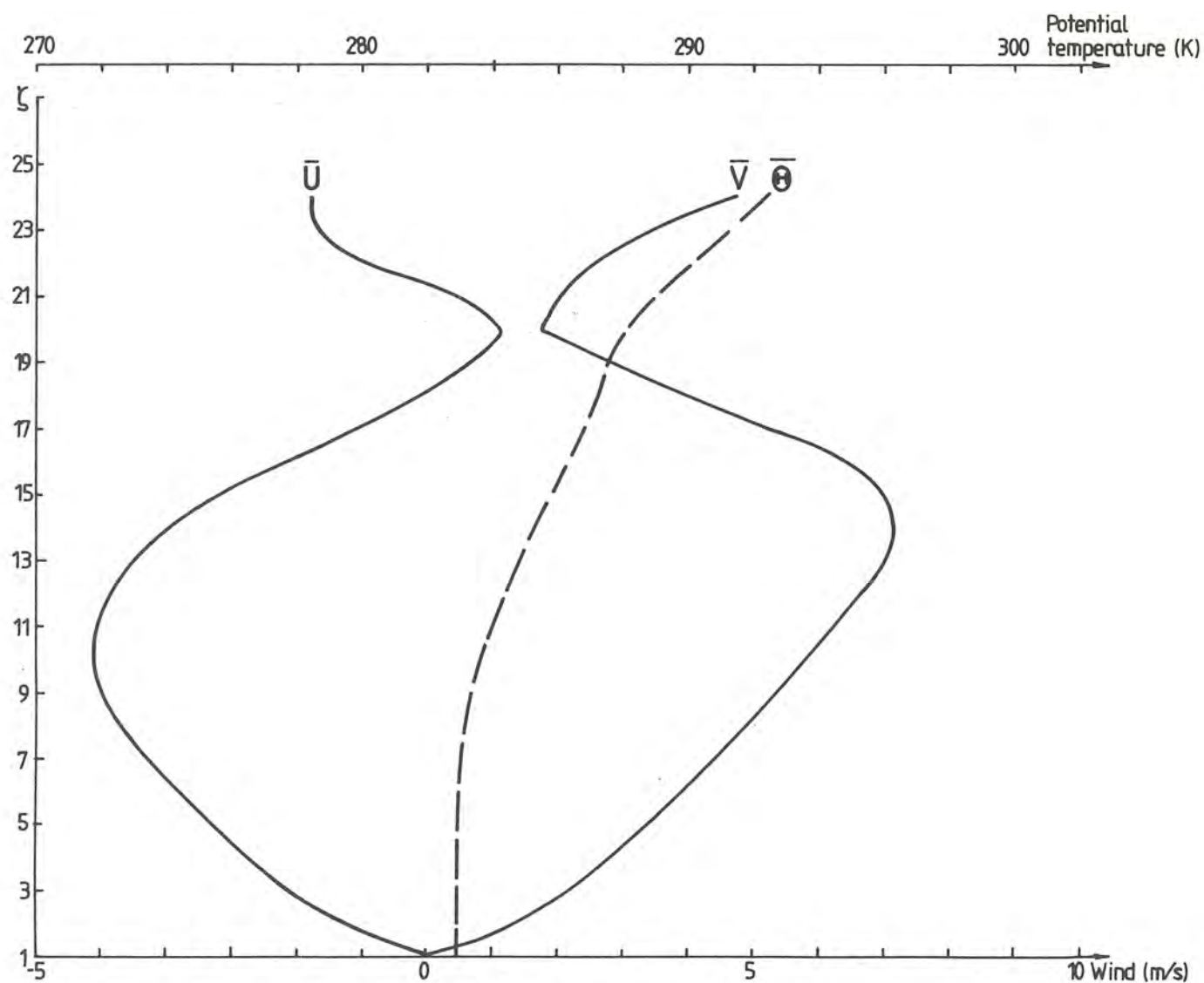
FIGURE 3. Profiles of the synoptic wind components $\overline{U}$ and $\overline{V}$ as well as potential temperature $\overline{\Theta}$.
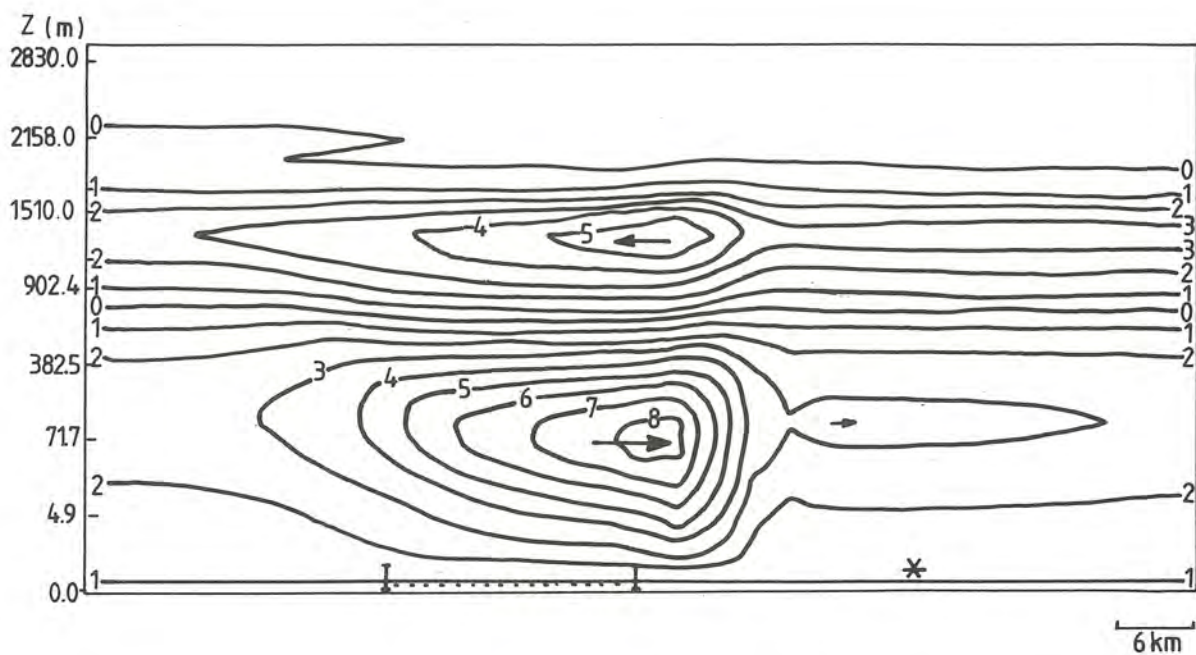
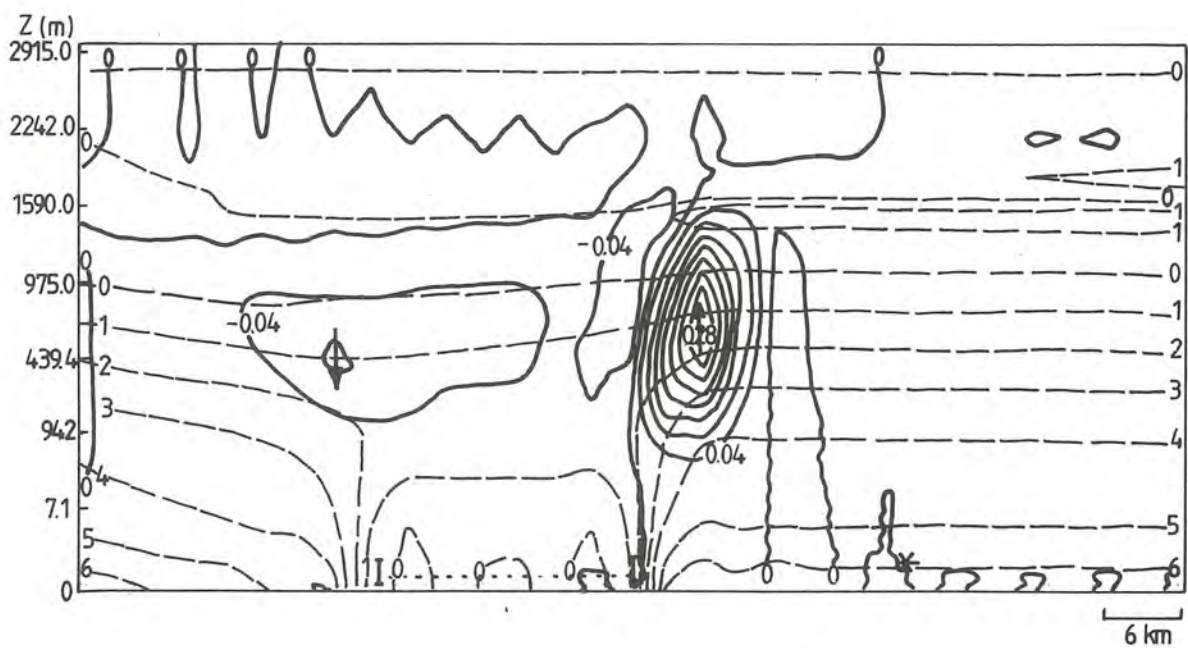FIGURE 4. u component of the mesoscale flow (m/s) at 1530 hours.

FIGURE 5. Vertical velocity (solid lines, m/s) and potential temperature difference between the air and the lake surface (dashed lines, K) at 1530 hours.
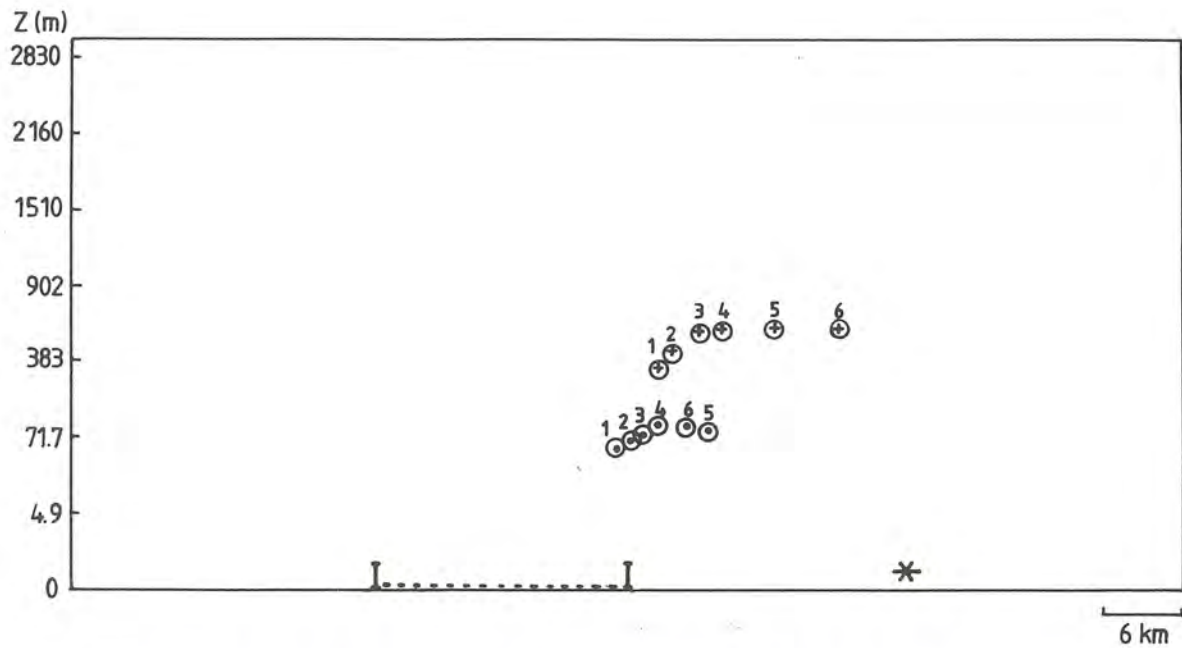
FIGURE 6. Variation in time of the location of the centers of the vertical velocity maximum '⊕' and of the centers of the lake breeze maximum 'O', which correspond to the eastern coastline; where the number 1 to 6, respectively, corresponds to the local time 1230, 1400, 1530, 1700, 1830 and 2000.
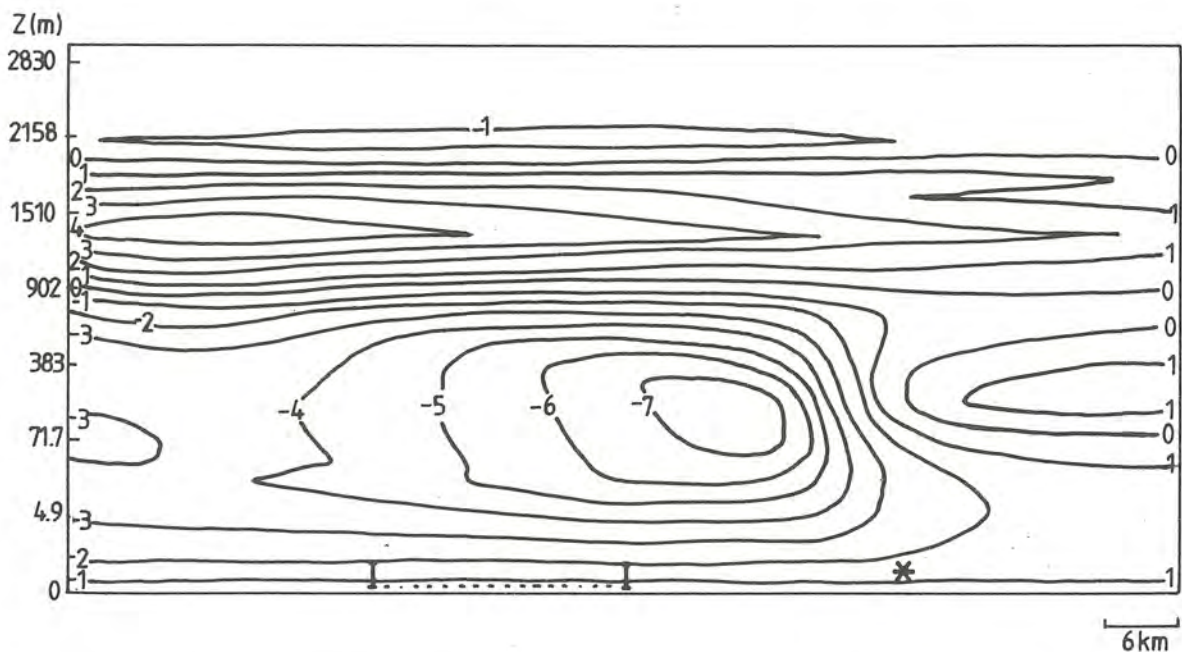

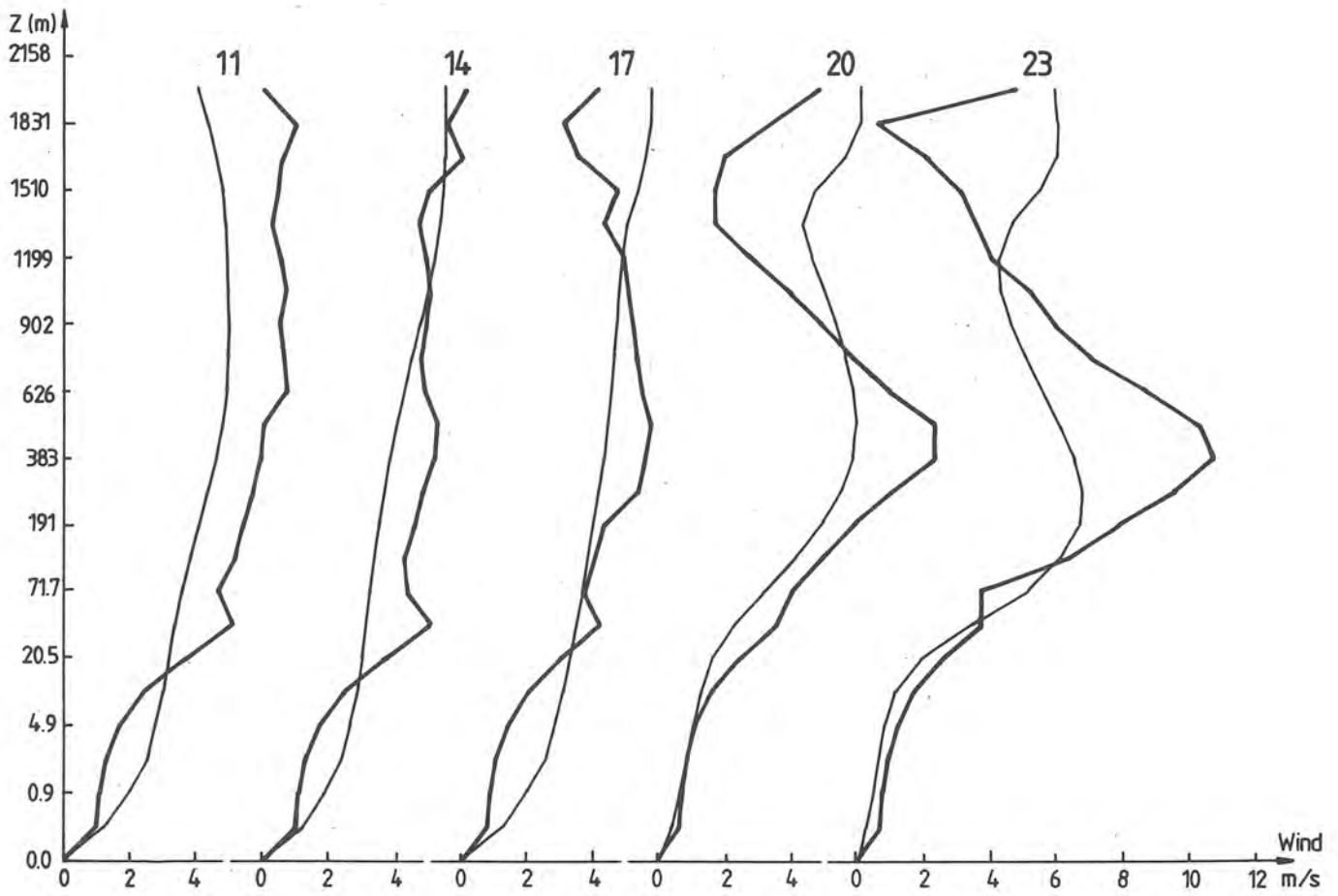FIGURE 7. v component field of the mesoscale flow (m/s) at 2000 hours.

FIGURE 8. Profiles of V component of wind speed at 11, 14, 17, 20, 23 hours, May 7, 1980 (at Klockrike). The thicker lines are the observed results, the thiner lines the calculated.
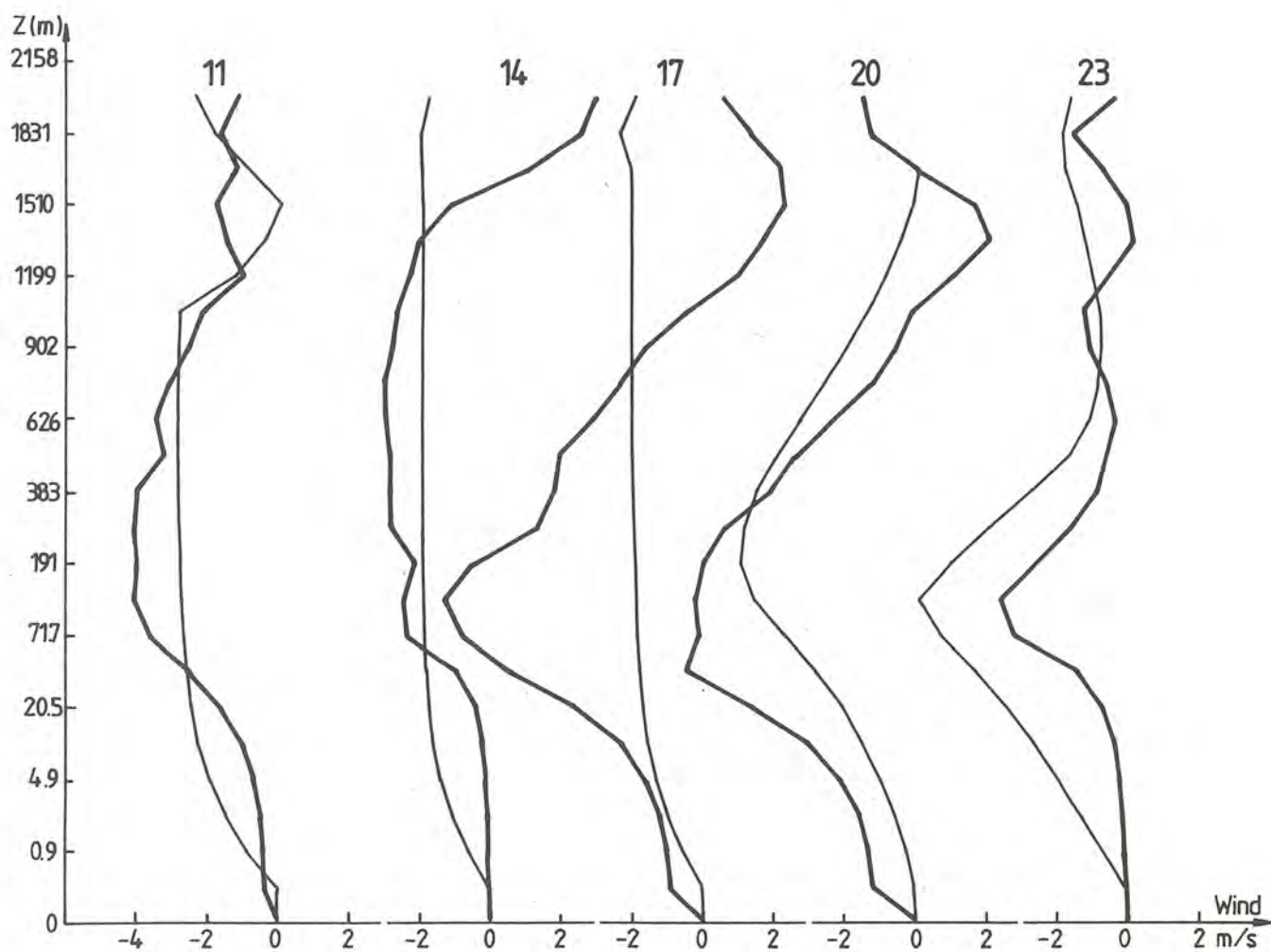
FIGURE 9. As the same as Fig. 8, but for U component of wind speed.

FIGURE 10. Inland penetration of the sea breeze of Physick's model plotted against time of day for different values of Bowen ratio β. Also shown is the average penetration curve for 76 sea – breeze fronts which passed Lasham, 1962 – 1973. (After Physick, 1980)

FIGURE 11. Schematic head of the inland lake breeze.

FIGURE 12. u component field of the mesoscale flow at lower levels (dashed lines, m/s) and potential temperature difference between the air and the lake surface (solid lines, K) at 0630 hours (a) on 7 and (b) on 8 May.

FIGURE 13. v component field of the mesoscale flow at 0630 hours on 8 May.
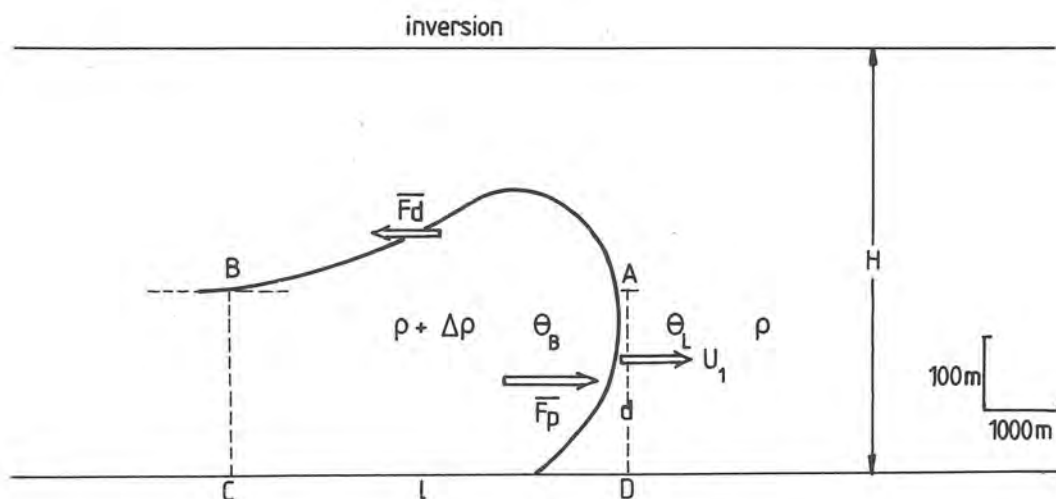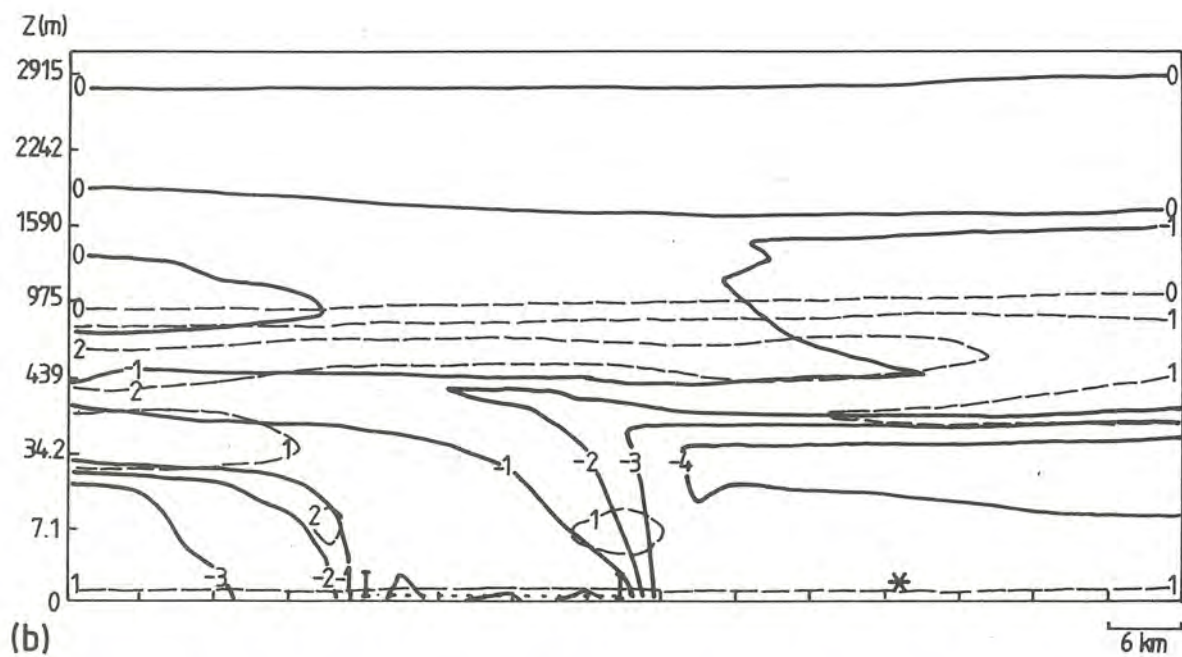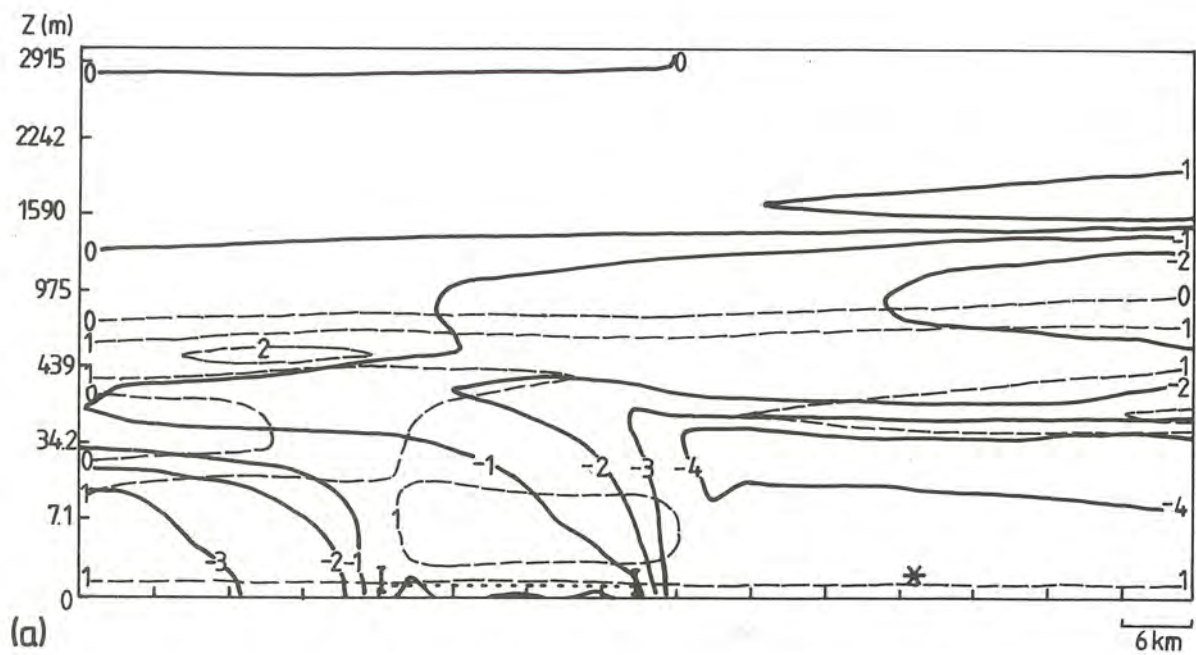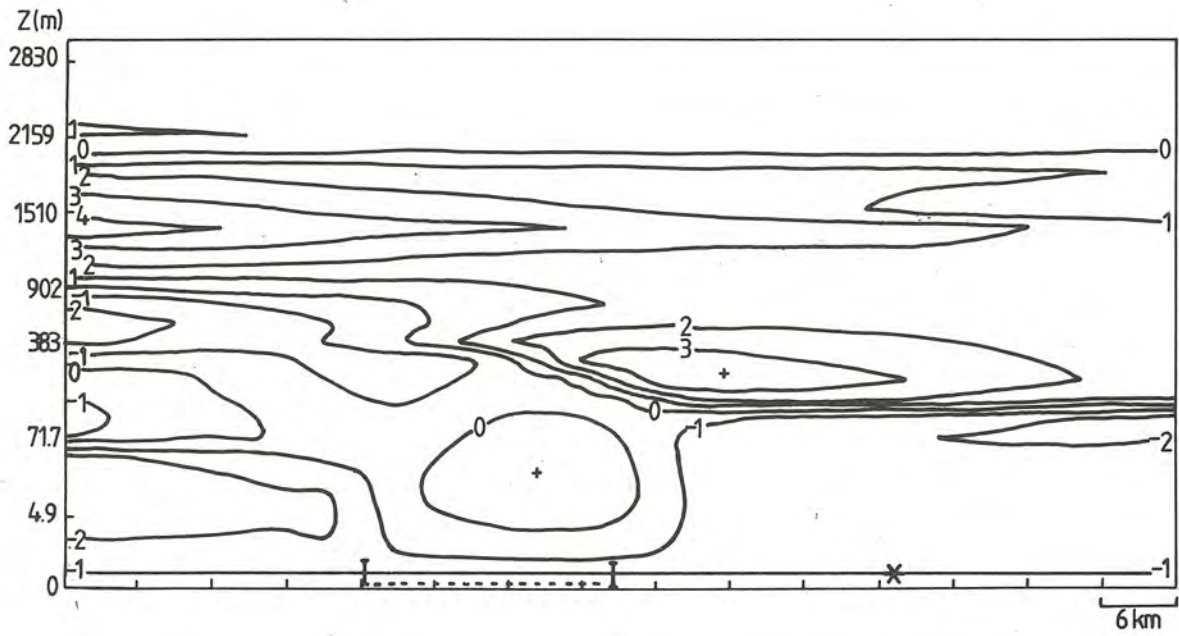
SMHI Rapporter, METEOROLOGI OCH KLIMATOLOGI (RMK)

Nr 1   Thompson, T, Udin, I, and Omstedt, A
        Sea surface temperatures in waters surrounding Sweden
        Stockholm 1974

Nr 2   Bodin, S
        Development on an unsteady atmospheric boundary layer model.
        Stockholm 1974

Nr 3   Moen, L
        A multi-level quasi-geostrophic model for short range weather
        predictions
        Norrköping 1975

Nr 4   Holmström, I
        Optimization of atmospheric models
        Norrköping 1976

Nr 5   Collins, W G
        A parameterization model for calculation of vertical fluxes
        of momentum due to terrain induced gravity waves
        Norrköping 1976

Nr 6   Nyberg, A
        On transport of sulphur over the North Atlantic
        Norrköping 1976

Nr 7   Lundqvist, J-E, and Udin, I
        Ice accretion on ships with special emphasis on Baltic
        conditions
        Norrköping 1977

Nr 8   Eriksson, B
        Den dagliga och årliga variationen av temperatur, fuktighet
        och vindhastighet vid några orter i Sverige
        Norrköping 1977

Nr 9   Holmström, I, and Stokes, J
        Statistical forecasting of sea level changes in the Baltic
        Norrköping 1978

Nr 10   Omstedt, A, and Sahlberg, J
        Some results from a joint Swedish-Finnish sea ice experi-
        ment, March, 1977
        Norrköping 1978

Nr 11   Haag, T
        Byggnadsindustrins väderberoende, seminarieuppsats i före-
        tagsekonomi, B-nivå
        Norrköping 1978

Nr 12   Eriksson, B
        Vegetationsperioden i Sverige beräknad från temperatur-
        observationer
        Norrköping 1978

Nr 13   Bodin, S
        En numerisk prognosmodell för det atmosfäriska gränsskiktet
        grundad på den turbulenta energiekvationen
        Norrköping 1979

Nr 14   Eriksson, B
        Temperaturfluktuationer under senaste 100 åren
        Norrköping 1979

Nr 15   Udin, I, och Mattisson, I
        Havsis- och snöinformation ur datorbearbetade satellitdata
        - en modellstudie
        Norrköping 1979

Nr 16   Eriksson, B
        Statistisk analys av nederbördsdata. Del I. Arealnederbörd
        Norrköping 1979

Nr 17   Eriksson, B
        Statistisk analys av nederbördsdata. Del II. Frekvensanalys
        av månadsnederbörd
        Norrköping 1980

Nr 18   Eriksson, B
        Årsmedelvärden (1931-60) av nederbörd, avdunstning och
        avrinning
        Norrköping 1980

Nr 19   Omstedt, A
        A sensitivity analysis of steady, free floating ice
        Norrköping 1980

Nr 20   Persson, C och Omstedt, G
        En modell för beräkning av luftföroreningars spridning och
        deposition på mesoskala
        Norrköping 1980

Nr 21   Jansson, D
        Studier av temperaturinversioner och vertikal vindskjuvning
        vid Sundsvall-Härnösands flygplats
        Norrköping 1980

Nr 22   Sahlberg, J and Törnevik, H
        A study of large scale cooling in the Bay of Bothnia
        Norrköping 1980

Nr 23   Ericson, K and Hårsmar, P-O
        Boundary layer measurements at Klockrike. Oct. 1977
        Norrköping 1980

Nr 24   Bringfelt, B
        A comparison of forest evapotranspiration determined by some
        independent methods
        Norrköping 1980

Nr 25   Bodin, S and Fredriksson, U
        Uncertainty in wind forecasting for wind power networks
        Norrköping 1980

Nr 26   Eriksson, B
        Graddagsstatistik för Sverige
        Norrköping 1980

Nr 27   Eriksson, B
        Statistisk analys av nederbördsdata. Del III. 200-åriga
        nederbördsserier
        Norrköping 1981

Nr 28   Eriksson, B
        Den "potentiella" evapotranspirationen i Sverige
        Norrköping 1981

Nr 29   Pershagen, H
        Maximisnödjup i Sverige (perioden 1905-70)
        Norrköping 1981

Nr 30   Lönnqvist, O
        Nederbördsstatistik med praktiska tillämpningar
        (Precipitation statistics with practical applications)
        Norrköping 1981

Nr 31   Melgarejo, J W
        Similarity theory and resistance laws for the atmospheric
        boundary layer
        Norrköping 1981

Nr 32   Liljas, E
        Analys av moln och nederbörd genom automatisk klassning av
        AVHRR data
        Norrköping 1981

Nr 33   Ericson, K
        Atmospheric Boundary layer Field Experiment in Sweden 1980,
        GOTEX II, part I
        Norrköping 1982

Nr 34   Schoeffler, P
        Dissipation, dispersion and stability of numerical schemes
        for advection and diffusion
        Norrköping 1982

Nr 35   Undén, P
        The Swedish Limited Area Model (LAM). Part A. Formulation
        Norrköping 1982

Nr 36   Bringfelt, B
        A forest evapotranspiration model using synoptic data
        Norrköping 1982

Nr 37   Omstedt, G
        Spridning av luftförorening från skorsten i konvektiva
        gränsskikt
        Norrköping 1982

Nr 38   Törnevik, H
        An aerobiological model for operational forecasts of pollen
        concentration in th air
        Norrköping 1982

Nr 39   Eriksson, B
        Data rörande Sveriges temperaturklimat
        Norrköping 1982

Nr 40   Omstedt, G
        An operational air pollution model using routine meteorologi-
        cal data
        Norrköping 1984

Nr 41   Christer Persson and Lennart Funkquist
        Local scale plume model for nitrogen oxides.
        Model description.
        Norrköping 1984

Nr 42   Stefan Gollvik
        Estimation of orographic precipitation by dynamical
        interpretation of synoptic model data.
        Norrköping 1984

Nr 43   Olov Lönnqvist
        Congression - A fast regression technique with a great number
        of functions of all predictors.
        Norrköping 1984

Nr 44   Sten Laurin
        Population exposure to SO_2 and NO_x from different sources in
        Stockholm.
        Norrköping 1984

Nr 45   Jan Svensson
        Remote sensing of atmospheric temperature profiles by TIROS
        Operational Vertical Sounder.
        Norrköping 1985

Nr 46   Bertil Eriksson
        Nederbörds- och humiditetsklimat i Sverige under vegetations-
        perioden
        Norrköping 1986

Nr 47   Roger Taesler
        Köldperioder av olika längd och förekomst
        Norrköping 1986

Nr 48   Wu Zengmao
        Numerical study of lake-land breeze over Lake Vättern
        Sweden
        Norrköping 1986

Nr 49   Wu Zengmao
        Numerical analysis of initialization procedure in a two-
        dimensional lake breeze model
        Norrköping 1986

SMHI